

# Integrated 3D Reservoir Modeling for the Delineation of Sand Body Geometry and Heterogeneity: Implication for Hydrocarbon Potential Assessment of “GMEDAL” Field, Offshore, Niger Delta

Oyesomi Hammed<sup>1</sup>, Bashir Koledoye<sup>1</sup>, Kunle Ajao<sup>2</sup>, Jude Ojero<sup>3</sup>, Christopher Jackson<sup>4</sup>, Oladele Sunday<sup>5</sup> and Adepelumi Adekunle<sup>6</sup>

<sup>1</sup>Dharmattan Nigeria Limited, Lagos, Nigeria.

<sup>2</sup>Chevron Nigeria Limited.

<sup>3</sup>The University of Manchester, UK.

<sup>4</sup>PetroVision Energy Nigeria Limited, Lagos, Nigeria.

<sup>5</sup>Department of Geosciences, University of Lagos, Akoka, Lagos, Nigeria.

<sup>6</sup>Department of Geology, Obafemi Awolowo University, Ile-Ife, Osun State, Nigeria.

## ABSTRACT

Reservoir architecture delineation and understanding of heterogeneity in geological reservoir models are crucial to accurately estimate hydrocarbon reserves, production forecast and recovery in an effective economic scenario. This study focused on delineation of sand body geometry and heterogeneity, geologic modeling and 3D static modelling for hydrocarbon potential assessment and detection of bypassed hydrocarbon that lead to volumetric enhancement in “GMEDAL” field, Offshore, Niger-Delta. 3D seismic data and well data containing six (6) wells were integrated to build structural, facies and petrophysical (total and effective porosity, permeability, net-to-gross, and water saturation) models using different geostatistical algorithms in Petrel software. Seventeen reservoirs (Sand 1-17) were identified and correlated. Petrophysical analysis was done using Techlog software and six most probable hydrocarbon bearing reservoirs were modeled. The saturation height function was used in populating the water saturation taking into cognizance the effect of capillary pressure built-up. The model geological cross section was constructed across the field in order to picture the reservoirs geometries and, the Gas-Oil-Contact and Oil-Water-Contacts. The structural modeling shows that fault dependent anticlinal structure dominated the field. Results of petrophysical analysis and modeling conditioned to facies models indicated porosity range of 5-30%, permeability between 300-9000milliDarcy, net-to-gross of 65%-98%, and water saturation of 5%-40%. The environments of deposition were inferred to be distributary channel, crevasse splay and shoreface systems based on well-log motifs and net-to-gross distribution maps. The volumetric figures were calculated, resulted in in-place volume range of 45 to 281mmmbbl. In conclusion, our investigation revealed that accurate description of internal reservoir geometry and heterogeneity play significant roles in hydrocarbon assessment, and “GMEDAL” field contains volumes of hydrocarbon that can be produced in commercial quantities.

**Keywords:** Static, Facies, Environment of Deposition, Anticlinal, Volumetrics, 3D Modeling, Shoreface, Crevasse Splay, Channel, Petrophysical, Algorithm, Geostatistical, Saturation Height Function, Geological Cross Section.

## INTRODUCTION

Three-dimensional geological reservoir modeling is not only the key factor for reservoir description and prediction of oil reserves but also important means quantitative characterization of reservoir geometry and heterogeneity in three-dimensional space, and its core is to predict hydrocarbon volumetric distribution within the reservoir. Therefore, reservoir modeling represents the

major focus hot topical issues in reservoir geoscience. Three-dimensional modeling of a reservoir is a process of selecting appropriate method to establish the structure, sedimentary microfacies, sand body geometry and reservoir petrophysical parameters on the bases of well logging, seismic and geological data.

Heterogeneity in reservoir study means the vertical and lateral variation in porosity, permeability and or capillarity. In the Niger Delta province of Nigeria, hydrocarbons are accumulated in the intercalated sand and shale of Agbada formation. The reservoir heterogeneity in sandstone body occur at various extent and scale ranging from micro meter to hundreds of meters and is commonly attribute to variation in depositional environment / facies, diagenesis, and structural features such as presence of fractures and faults (De Ros *et al.*, 1998). Therefore,

© Copyright 2020, Nigerian Association of Petroleum Explorationists.  
All rights reserved.

The authors wish to thank the management of Dharmattan Nigeria limited and Department of geoscience, University of Lagos for their support during the course of this project. We also wish to thank Department of Petroleum Resources for authorizing one of the oil company to release the data used for this research.

NAPE Bulletin, Vol. 29 No 1, April 2020 (ISSN: 2734-3243) P. 89-107

elucidating and prediction of reservoir heterogeneity are of prime importance for the planning and execution of efficient hydrocarbon production strategies (Sech *et al.*, 2009). The heterogeneity pattern of sandstone reservoirs determines the volume, flow rate and recovery of hydrocarbons are controlled by geometry and internal structure of sand bodies, grain size, degree of bioturbation, provenance and by the type, volume and distribution of diagenetic alteration.

Fluvial sandstone reservoirs contain some of the highest percentage of unrecovered mobile hydrocarbons within known reservoirs due to inherent complex internal depositional architecture and heterogeneity. Gmedal field is one of the most prolific hydrocarbon fields located in the shallow offshore of the Nigerian Niger Delta basin and the hydrocarbon within the field has not been optimally produced. This study therefore focused on delineation of sand body geometry and heterogeneity, geologic modeling and 3D static modelling for hydrocarbon potential assessment and detection of bypassed hydrocarbon that lead to volumetric enhancement in "GMEDAL" in order to provide a reference model of oil reserve prediction in the area and development of reservoirs parameters in the adjacent areas of the Niger Delta basin.

## **GEOLOGY AND LOCATION OF THE STUDY AREA**

### **Geology of the Niger Delta**

The study area is in the Niger delta basin (Figure 1a) which formed along a failed arm of a triple junction system (aulacogen) that originally developed during the breakup of the South American and African plates in the late Jurassic, (Burke *et al.*, 1972). It is located between latitude 3° N to 6° N and longitude 4° E to 9° E. It covers a total area of 105,000 km<sup>2</sup> (Avbovbo, 1978). It extends in an East – West direction from South West Cameroun to the Okitipupa Ridge. It apex is situated southeast of the confluence of the Niger and Benue rivers. It lies mainly in the Gulf of Guinea to the southwest of the Benue trough. It is bounded in the north by Anambra basin, Abakaliki uplift, Afikpo syncline and in the south by Gulf of Guinea.

According to Short and Stauble (1967), Niger River carries estimated 2.62 X 10<sup>6</sup> m<sup>3</sup> of sand out of which 35% reach the sea while the rest are trapped in the delta. The delta is subjected to strong and persistent tidal action and marine current which divert the sediments, distribute them along the coast, and thus lead to formation of an arcuate-shaped delta (Figure 1b)

Multidisciplinary studies carried out in the area of Niger Delta reveal that the modern Niger Delta is built on an oceanic crust (Burke *et al.*, 1972). The Tertiary Niger

Delta consists of outcrops and subsurface formations. The outcrop formations include the Paleocene marine Imo Shale, Ameki Formation, Ogwasi Asaba Formation, Benin Formation while the subsurface formations are Akata, Agbada and Benin Formations in ascending order (Doust and Omatsola, 1990).

### **Akata Formation**

The formation is characteristically uniform shale development and occurs at the base of the Tertiary Niger Delta sequence (Figure 1b). It consists of marine shale that is dark-gray in colour, fairly hard, gumbo like and sandy or silty beds which were thought to be continental slope channel-turbidites (Short and Stauble, 1967; Weber & Daukuro, 1975). The shale is under compacted and may be of abnormally high pressure. The formation was estimated to be seven thousand meters (7000 m) in thickness (Doust and Omatsola, 1990). Turbidity currents likely deposited deep sea fan sands within the upper Akata Formation during development of the Delta (Burke *et al.*, 1972). Based on the foraminifera content, Akata Formation was considered the oldest in the Niger Delta and dated Eocene to Recent. It has been suggested to be source rock for oil and gas in the Niger Delta (Short and Stauble, 1967).

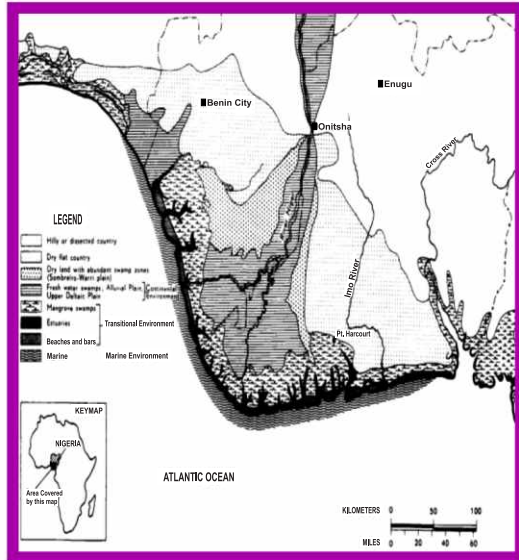
### **Agbada Formation**

The formation underlies the Benin Formation and overlies Akata Formation (Figure 1b). It consists of alternating sequence of sandstone and shale of delta front, distributaries channel, and of deltaic-plain origin suggested to be a cyclic sequence of marine and fluvial deposit. The sandstones are medium to fine grained, fairly clean, shelly and calcareous. It consists of quartz, potash feldspar, plagioclase, kaolinite and illite. The shale is medium to dark gray, fairly consolidated, locally silty and glauconitic. The formation has maximum thickness of 3940m and thins northward and towards northwestern and eastern flank of the delta. The sandstone of the Agbada Formation constitutes the hydrocarbon reservoir while the shale serves as cap and source rock because of its high organic content. The age of the formation ranges from Eocene in the north to Pliocene in the south. The Formation is the main exploration target for oil companies in Southern Nigeria since it forms the main reservoir of the hydrocarbon and contains growth faults and rollover anticlines formed along these faults, which trap hydrocarbons, (Evamy *et al.*, 1978).

### **Benin Formation**

This formation overlies the Agbada Formation and is the topmost of the Tertiary Niger Delta (Figure 1b). It consists of massive, highly porous freshwater bearing sandstone with local shale interbeds considered to be of braided stream origin. Mineralogically, the sandstone consists dominantly of quartz, potash feldspar and minor amount of plagioclase. The maximum thickness of the formation

is 1970 m and corresponds to the depocenter of Agbada Formation. Composition, structure and grain size of the sequence indicate that the deposition of the formation is continental probably upper deltaic environment. The age of the formation varies from Oligocene to Recent.



The base map of the study area is shown in figure 2.

## METHODOLOGY

### Petrophysics:

**Well log analysis:** After data gathering and QC, the first

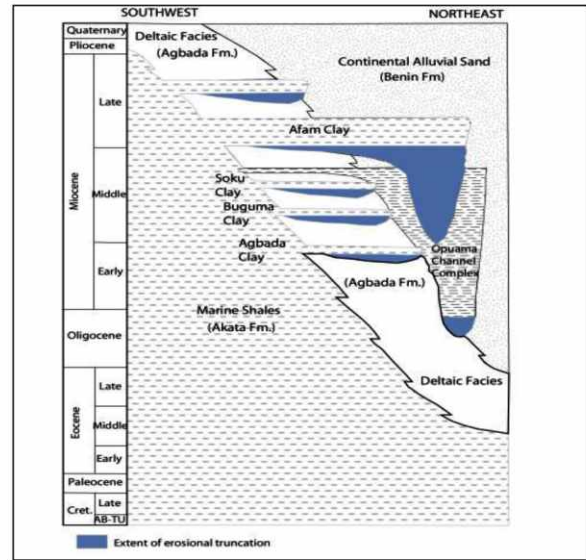


**Figure 1a:** Map of southern Nigeria showing Location of study area and **Figure 1b:** The stratigraphy of Niger Delta (After Doust and OmatSola, 1990).

## MATERIALS AND METHODOLOGY

**MATERIALS:** The data used for this research comprise of 3D seismic data covering an area of about 59336.4 acres and suites of composite well logs (GR, ILD, NPHI, RHOB), deviation data, and check-shot data from six (6) wells (GMEDAL 04, 05, 011, 021 and GMEDAL 032).

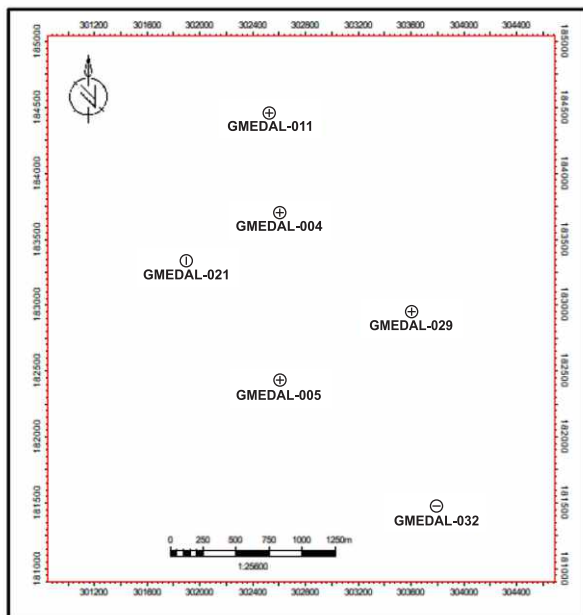


**Figure 2:** Base Map of the study area.

approach in this project was petrophysical analysis which involve gross lithologies delineation in each well based on the alternating deflection of GR log, Resistivity, density and neutron porosity signatures on Techlog software. Structural and stratigraphic lithologic correlation was carried out in order to establish the lateral extent of the reservoirs within GMEDAL Field. (Figure 3a).

### Shally sand analysis

The shally sand analysis was carried out for all the reservoir of interest in order to understand the shale distribution within reservoir of interest and to arrive at the best method to be used in petrophysical parameter computation and analysis. Thomas Steiber graphical method of shally sand analysis was adopted and it revealed that dispersed and laminated shale distribution characterized / dominated the field.

### Computation of petrophysical Parameters

Petrophysical parameters such as Volume of Shale ( $V_{sh}$ ), Permeability ( $K$ ) computed using Willie Rose and coat methods, Effective and total Porosity ( $\phi_e$  &  $\phi_t$ ) Bulk Volume of Water (BVW) and Water saturation computed using modified Simandoux and Indonesian methods ( $S_w$ ) were all carried out on Techlog Software 2015 version. The  $R_o$  (Resistivity of the water bearing Zone) used in the water saturation computation was determined using Picket Plot and Apparent water resistivity ( $R_{wa}$ ) and both



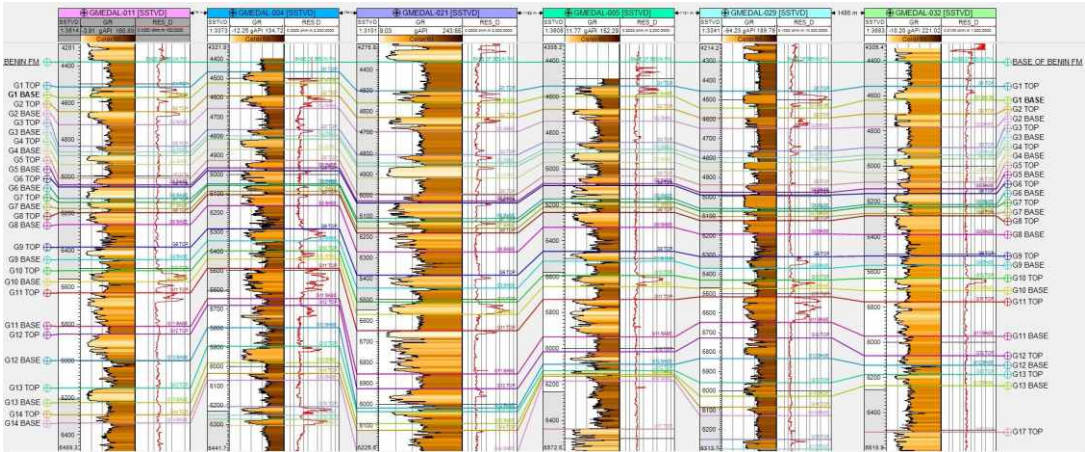


Figure 3a: Lithology correlation across six wells in GMEDAL field.

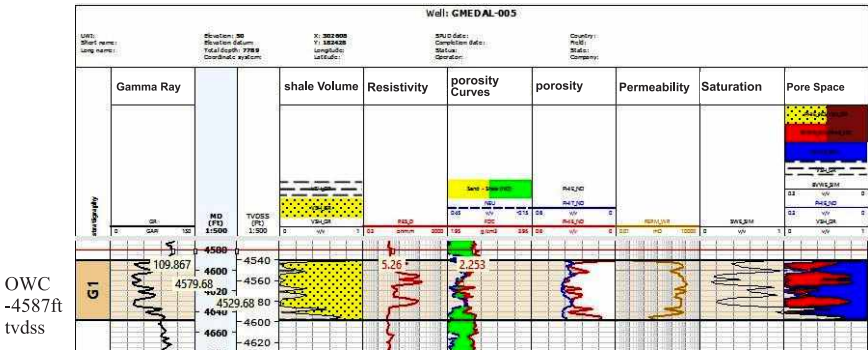


Figure 3b: Petrophysical evaluation log-plot of sand G1.

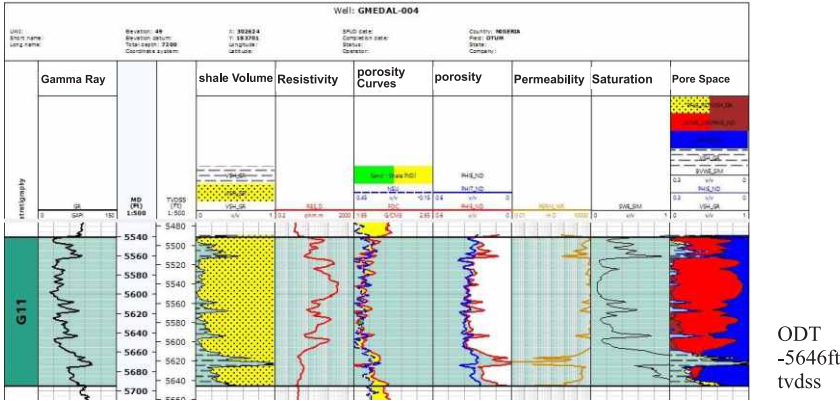


Figure 3c: Petrophysical evaluation log-plot of sand G11.

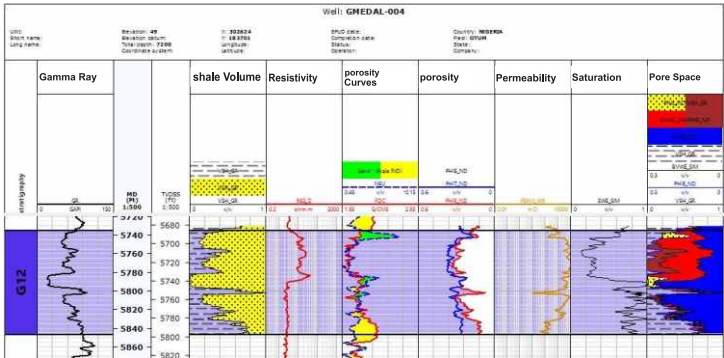
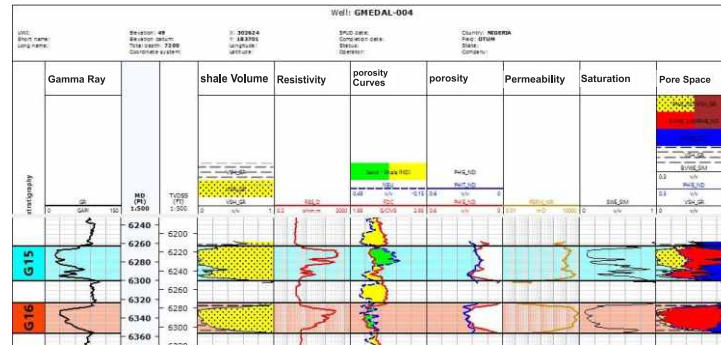


Figure 3d: Petrophysical evaluation log-plot of sand G12.





**Figure 3e:** Petrophysical evaluation log-plot of sand G15 & G16.

values gave similar results (Figure 3b-e).

### Cut off determination

The various cut offs used in the pay summary computation was determined on the sensitivity analysis that was carried on Techlog software and also based on regional knowledge. We then arrive at the following cut offs.

Vsh cut off 0 – 0.6,  $\phi_e$  cut off 0.05 – 0.40 and Sw cut off 0 – 0.60

### Saturation Height Function (SHF)

In order to mitigate against the capillary pressure built up within the field, saturation height function was generated on Techlog using height above free water level (HAFWL) in all the hydrocarbon probable reservoir within the study area. The SHF helps predict saturation anywhere in the reservoir for a given height above free water level and effective porosity. The output function from each reservoir was used in the 3D model of water saturation.

### Fluid Discrimination

Fluids within delineated sand units were discriminated on deep resistivity log, and on the crossover between Density-Neutron porosity logs. Reservoir unit with high resistivity reading are interpreted as probable hydrocarbon bearing while sand units with low resistivity reading were interpreted as water-bearing reservoirs. Neutron and Density porosity logs crossover was used for Hydrocarbon type delineation. Oil-Down-To (ODT), Gas-Oil-Contact (GOC), Oil-Water-Contact (OWC) and Water-Up-To (WUT) were all delineated and incorporated into the 3D model built (Figure 3b-e)

### Seismic Data Analysis

3D Seismic data consisting of Inline, cross-line and Time slice was analyzed on Petrel software 2017 version.

### Faults and Well-to-seismic tie

The structural pattern within the field by running variance edge and structural smoothening volume attribute on the 3D seismic volume. These attribute aided in fault identification and mapping Figure 4a-4c. The Well-to-Seismic was done using check-shot data in GMEDAL 04,

05, 011, 021 and GMEDAL 032. Delineated reservoir tops were then displayed on seismic section and corresponding seismic events were mapped manually on inline and cross line with a bin spacing of 8.

### Fault polygon, Time & Depth structure Map

Polygons were constructed round faults on the mapped horizon and were then eliminated during the make surface process to produce time structure maps. The check-shot of “Gmedal” 04 well was used in generating the 3rd degree polynomial function that was used in converting time structure maps to depth domain.

### Isochore Map

The thickness maps were generated for all the reservoir of interest in order to capture the variation in thickness on a map scale. These serve as input in reservoir base map generation and also provide information that was used in layering process during static modeling. The average reservoir thickness deduced from isochore maps generated ranges from 66ft in G1 to 199ft in G11 reservoirs.

### Measurement of Heterogeneity

Geo-statistical tool was deployed in quantification of heterogeneity from the computed petrophysical parameters within the study area. Detailed coefficient of variation of computed effective porosity and modeled effective porosity was carried out to determine the degree of reservoir intra-formational heterogeneity within GMEDAL field. The degree of reservoir heterogeneity was classified using standard reservoir heterogeneity classification.

### 3D Geologic Reservoir Model

The reservoir geological modeling was carried out to establish an attribute model that reflect the characteristics of subsurface reservoir (sand body geometry, porosity, permeability, NTG and Saturation) spatial distribution in order to represent as closely as possible the subsurface reality of GMEDAL field reservoirs. The 3D model was built by integrating relevant subsurface information and data. Results of seismic interpretation, lithology

description, facies interpretation, petrophysical analysis (Effective porosity, permeability, water saturation, net-to-gross) were all encapsulated to build the 3D model in Petrel 2017 version.

### **Grid design**

The grid size determination plays an important / crucial role in the resolution and size of the model, well spacing density, reservoir vertical and lateral heterogeneity resolution of thickness of single layer well data and sampling density were all considered because the grid and cell size determine the time necessary for running reservoir simulation. The grid cells were set at 100 \* 100 \* 1 along I, J and K respectively considering the areal extent of the field to be 59336.4 acres and thickness of reservoir that ranges from 66ft in G1 to 199ft in G11 reservoirs.

### **Structural Model**

The structural model built was based on Depth converted structural maps generated from 3D seismic interpretation. Tops and bases depth maps and fault polygons also serve as input into building the structural model. Fault modeling was then carried out in order to structurally and geometrically positioned faults along fault polygons in the model horizons. Pillar gridding was then followed to generate top, mid and base skeletons of the 3D grid framework. The final step in building the 3D grid structural framework is layering which is the process of defining the thickness and orientation of layers between zones within the grid. These layers coupled with pillars define the cell size of the 3D grid that are assigned properties during property modeling. Each zone within the field was divided into different number of layers of 1ft thickness.

### **Scale up well logs**

The scale up well logs process averages the values of the logs penetrated by wells to the cells in the 3D grid. Each cell gets one value per up-scaled log. These cells are later used as a starting point for property modeling (Schlumberger, 2013). When modeling petrophysical property, a 3D grid cell structure is used to represent the volumes of the zones. The cell thickness will normally be larger than the sample density for well logs. As a result, the well log must be scaled up to the resolution of the 3D grid cells before any modeling based on well logs can be done. This process is also called blocking of well logs. The scale up of effective porosity, permeability, water saturation, NTG, facies were done and they serve as input in the petrophysical modeling.

### **Variogram analysis**

A variogram is a plot of variability in terms of semi-variance against separation distance in a specific direction. It is a key parameter used by most of geostatistical property modeling algorithms to describe that natural variation in the property. Horizontal variogram was

generated from depth structural maps and sample variogram model was built from where the major, minor and orientation were determined as 3000, 2400 and -40 degree respectively. These values were then used as part of input in facies and petrophysical modeling.

**Facies modeling:** Litho-Facies modeling is very crucial in modeling process with sole purpose of simulating sand bodies in the formation. The GMEDAL field composed of sand, silt and shale. These were trend using the vertical proportion curves output in order to accurately represent the geology of the field. The facies cut offs was defined using petrel syntax. Sequential Indicator Simulation (SIS) algorithm was used to model all the defined zones within the study area. The chosen algorithm is a stochastic method that combines variogram and target volume fraction, and it's suitable in modeling facies environment where facies volume proportion vary vertically, laterally or both.

### **Petrophysical modeling**

Petrophysical (net-to-gross, effective porosity, and permeability) models were built using Sequential Gaussian Simulation method of geo-statistics. The scale up of net-to-gross, effective porosity, and permeability, major and minor range of anisotropy and orientation were used as input petrophysical modeling. The petrophysical models were conditioned to facies models earlier built. Saturation height function (SHF) generated from Techlog was used in populating water saturation in order to mitigate against capillary pressure built up. Different function generated from different reservoirs were used to characterized the saturation of GMEDAL field.

### **Volumetrics**

The original oil in place (OOIP) was computed for all the interpreted reservoir of interest (G1, G2, G9, G10, G11 and G12) within GMEDAL Field using the net to gross, effective porosity and water saturation model as input.

$$OOIP = 7758 \times GRV \times NTG \times \phi_e \times (1 - sw)$$

Where

GRV=Gross Rock Volume (Area in Acres \* Thickness in Feet), NTG= Net-To-Gross,  $\phi_e$ = Effective Porosity, and Sw= Water saturation, 7758=Acre-Feet conversion for oil.

### **Sedimentary microfacies**

The environment of deposition within the study area was determine from the GR log motifs and NTG maps of all the reservoirs of interest. This was due to lack of core and biostrat data in the field.

## **RESULT AND DISCUSSIONS**

### **Results**

The result of seventeen correlated reservoirs and petrophysical analysis across the six well in GMEDAL



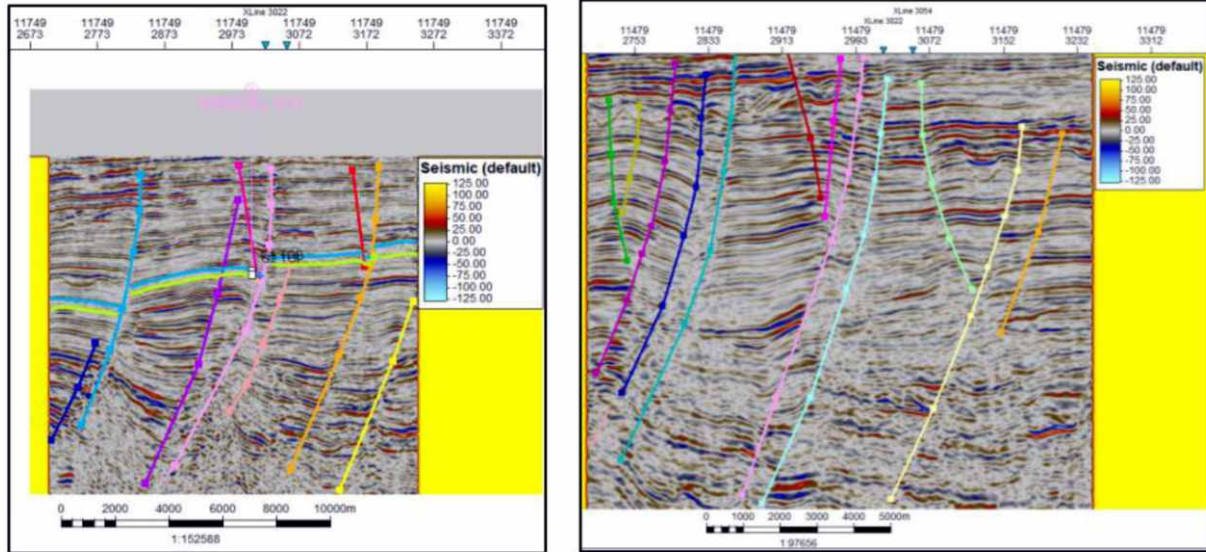


Figure 4a & b: Well-to-seismic tie, faults and Horizon mapping.

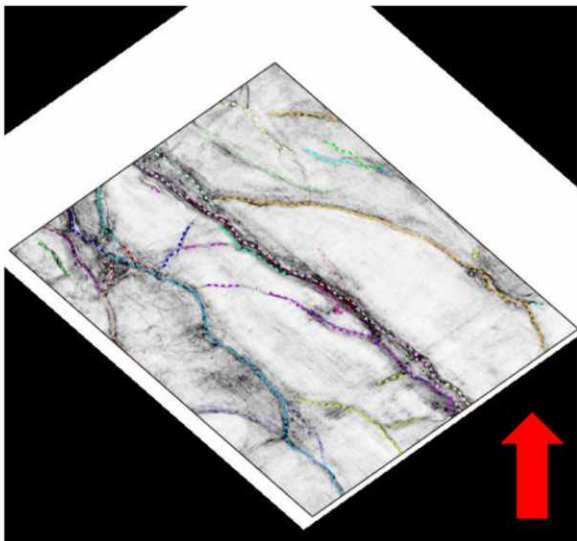


Figure 4c: Variance edge attribute and interpreted faults.

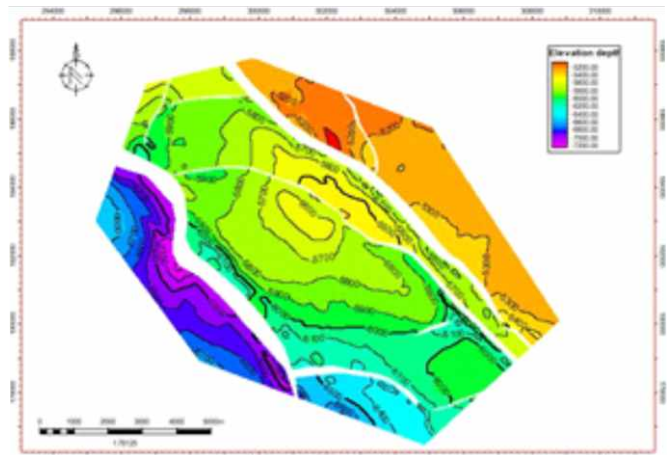


Figure 5b: Flexed top Structure depth map of reservoir G11.

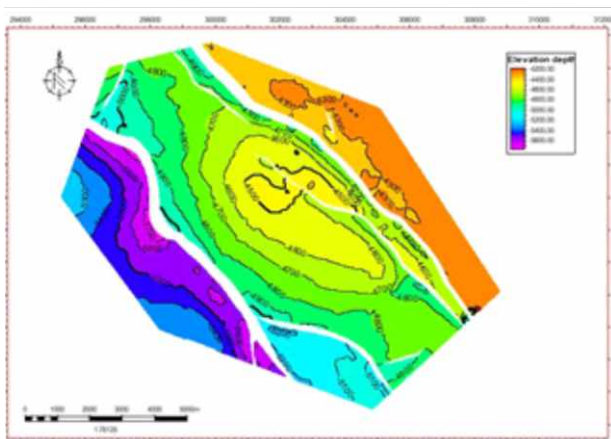


Figure 5a: Flexed top Structure depth map of reservoir G1.

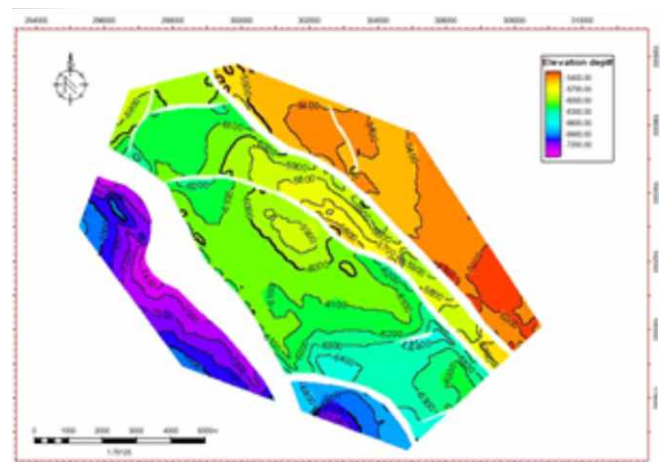


Figure 5c: Flexed top Structure depth map of reservoir G12.



field is displayed in Figure 3a. The structural smoothing, variance edge attribute, well to seismic tie and horizon mapping were displayed in Figure 4a-c. The flexed top depth maps were displayed in figure 5a-c. The 3D grid component is displayed in figure 6a and 6b, facies model in figure 8a and b, petrophysical models (NTG, Porosity, and Permeability) were displayed in figure 9, 10 and 11 respectively. The porosity coefficient of variation from both petrophysical analysis and 3D geological models were displayed in figure 12. The log motifs were displayed in figure 3a-3d and NTG map is captured in figure 7 while the OOIP and reserve were displayed in figure 13.

## DISCUSSION OF RESULTS

### Petrophysical analysis

The wells GMEDAL 04, 05, 011, 021, 029 and 032 were drilled to a total depth of 7148ft, 7704ft, 7454ft, 6571ft, and 7080ft SSTVD respectively. The GMEDAL 04 and 021 are wildcat while GMEDAL 05, 021, 029 and 032 were appraisal wells. They all contain basic suites of well logs that was used in this project/study. Seventeen reservoirs G1 to G17 were identified and correlated across the six wells in order to establish the lateral continuity of the sand body package and their thickness / vertical variation within the field. The net sand thickness varied from 27ft in G3 and G16 reservoir to 146ft in G11 reservoir. Reservoir G1, G2, G3, G9, G10, G11, G13, G16, were all oil bearing, reservoir G4, G6, G7, G8, G12 and G15 are oil and gas bearing while G5, G14, and G17 are wet reservoirs. GMEDAL 04, 011, 021, and 029 wells saw ODT in reservoir G1 at 4524ft, 4572ft, 4559ft, and 4540ft SSTVD respectively while GMEDAL 05 and 032 saw OWC at same depth of 4586ft SSTVD. The G2 reservoir has an ODT at 4658ft SSTVD in GMEDAL 04, 4645ft SSTVD in GMEDAL 029, and has OWC at 4675ft SSTVD in GMEDAL 011 and 4656ft SSTVD in GMEDAL 021. The difference in OWC observed in G2 reservoir indicated that GMEDAL 011 and GMEDAL 021 wells are in different compartment. This will be further buttress in other analysis.

GOC and OWC of 4873ft and 4878ft SSTVD occurred at reservoir G4 in well GMEDAL 021 and was wet in other wells. Reservoirs G6, G7, and G8 have Oil-Water-Contact at 4996ft, 5070ft and 5119ft SSTVD respectively in GMEDAL 04 well, Gas-Water-Contact at 5052ft SSTVD, 5143ft, and 5189ft SSTVD respectively in GMEDAL 021 well and are wet in other wells.

GMEDAL 04 saw an Oil-Down-To at 5345ft, 5440ft, and 5646ft SSTVD in reservoir G9, G10, and G11 respectively while GMEDAL 021 saw an Oil-Water-Contact at 5403ft SSTVD in G9, ODT in reservoir G10 at 5570ft SSTVD, and OWC at 5665ft in reservoir G11. Reservoir G12 has a GOC and OWC at 5696ft and 5741ft SSTVD respectively in GMEDAL 04, OWC at 5966ft in GMEDAL 021 and is

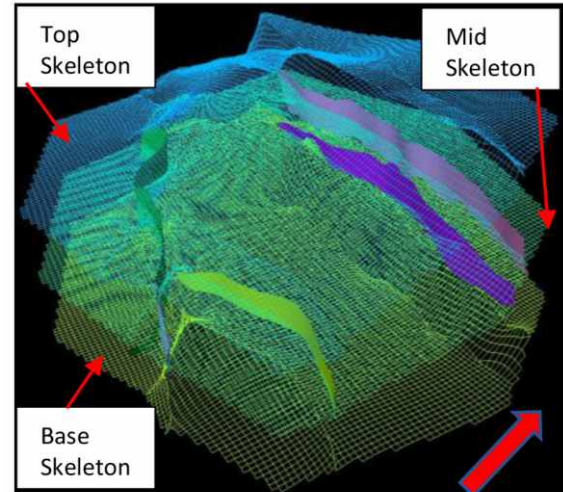


Figure 6a: 3D grid component of reservoir G1.

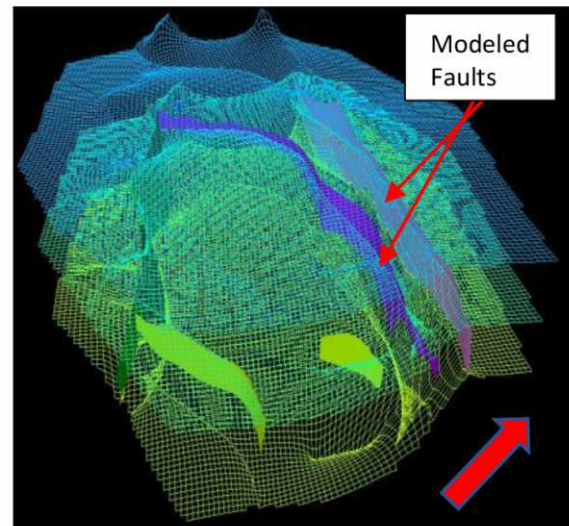


Figure 6b: 3D grid component of reservoir G11.

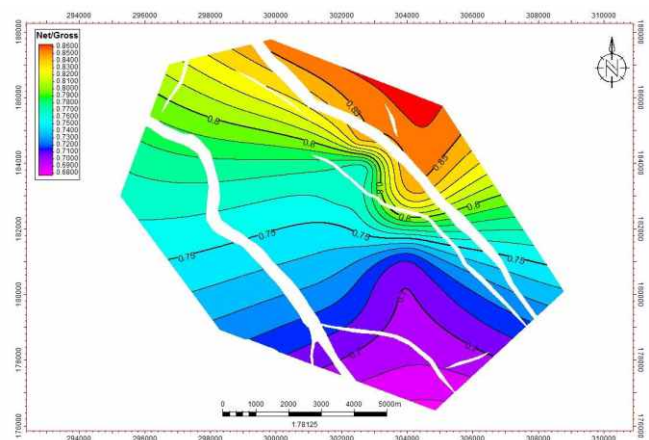
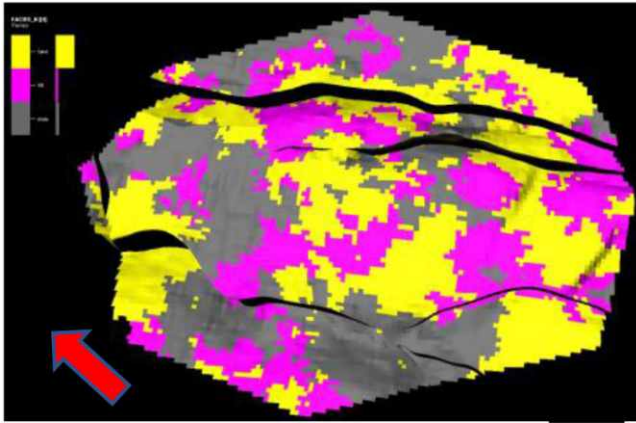
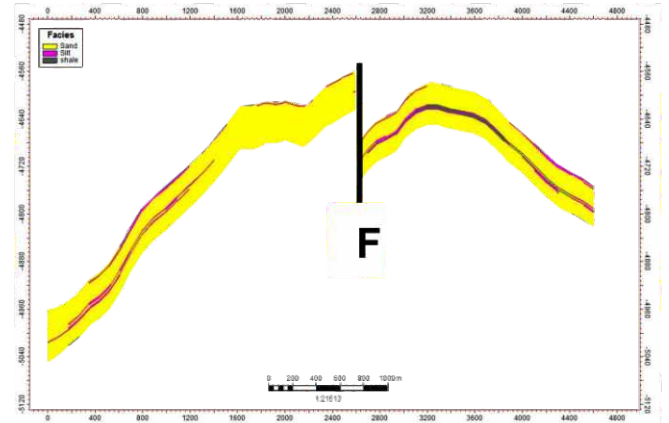


Figure 7: NTG map of reservoir G2.



**Figure 8ai:** Facies model of reservoir G1.



**Figure 8bii:** Facies model cross section of reservoir G2.

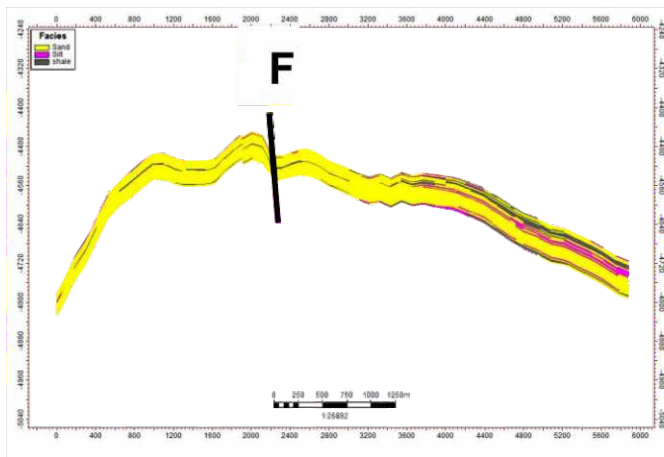


**Figure 8aii:** Facies model cross section of reservoir G1.

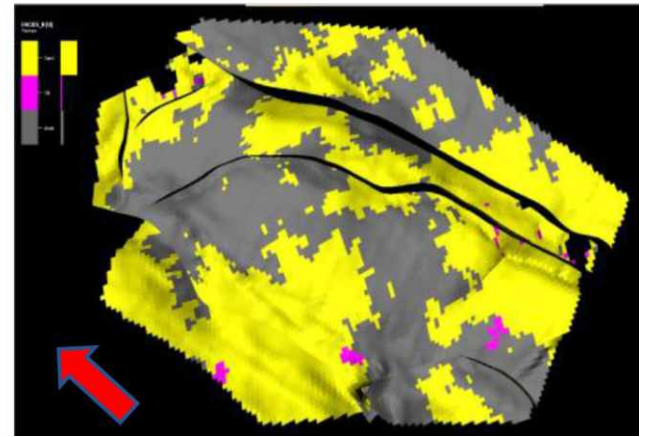


**Figure 8ci:** Facies model of reservoir G10.

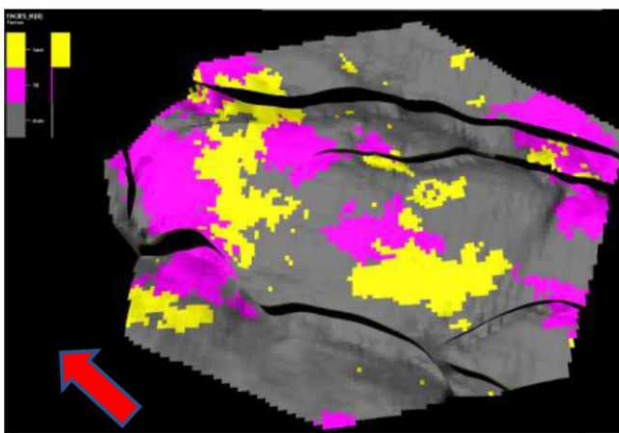


**Figure 8bi:** Facies model of reservoir G2.

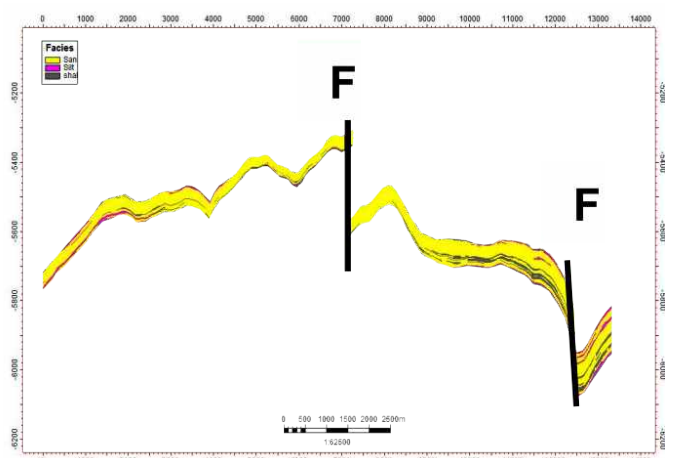


**Figure 8cii:** Facies model cross section of reservoir G10.



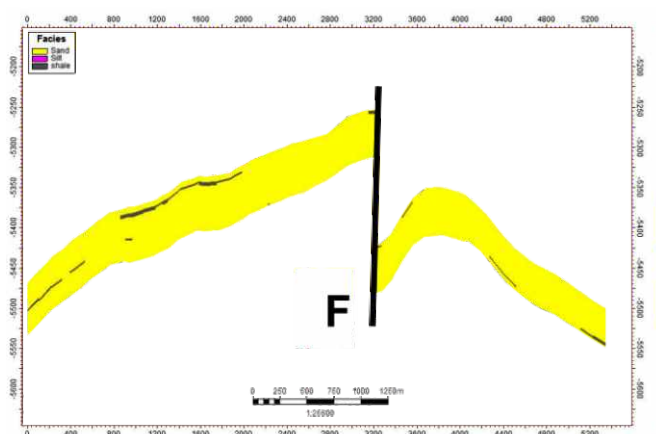


Figure 8dii: Facies model cross section of reservoir G9.

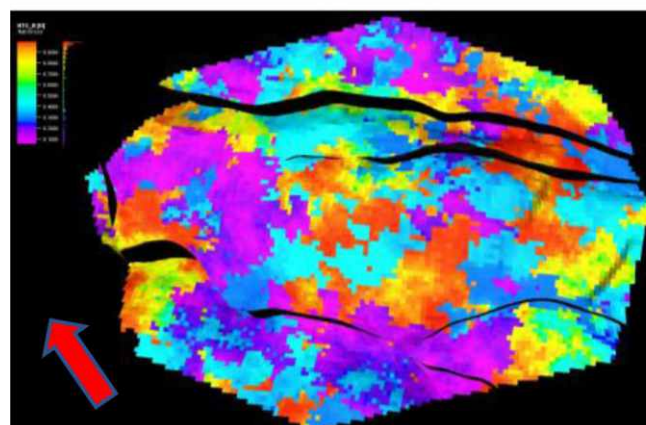


Figure 9ai: NTG model of reservoir G1.

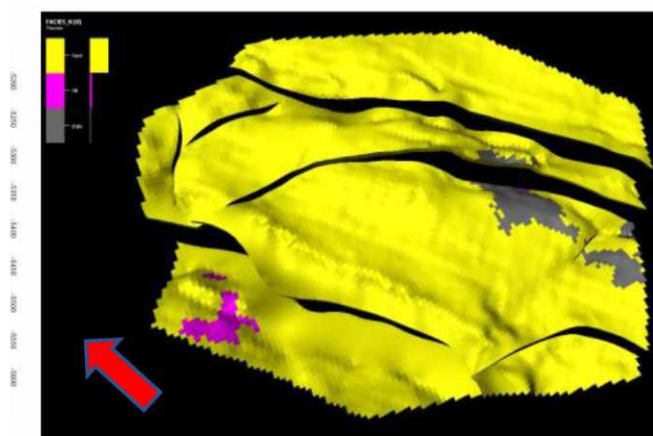


Figure 8ei: Facies model of reservoir G12.

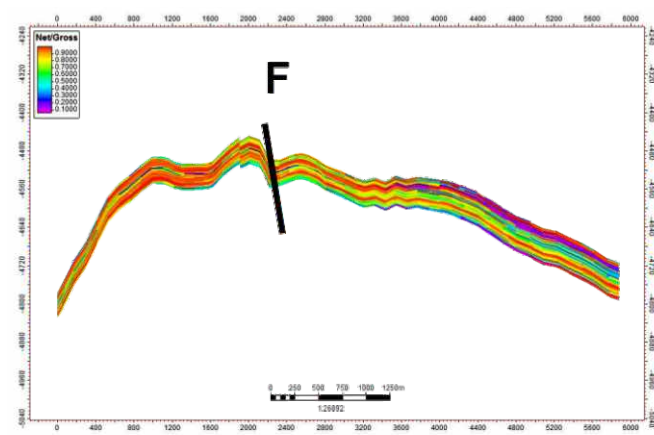


Figure 9aii: NTG model cross section of reservoir G1.

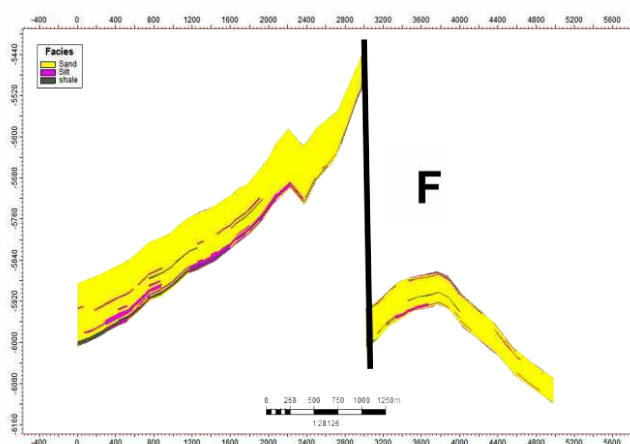


Figure 8eii: Facies model cross section of reservoir G12.

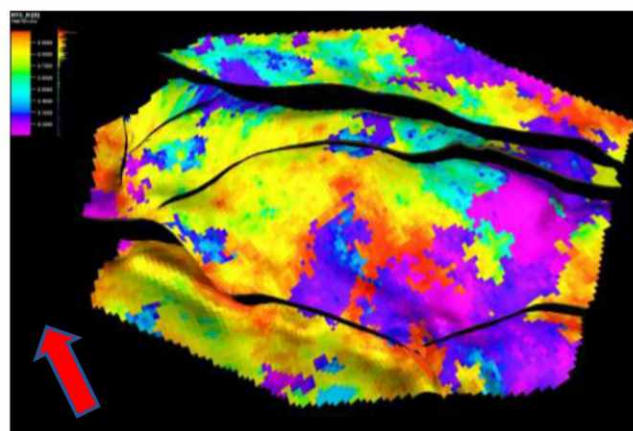


Figure 9bi: NTG model of reservoir G9.



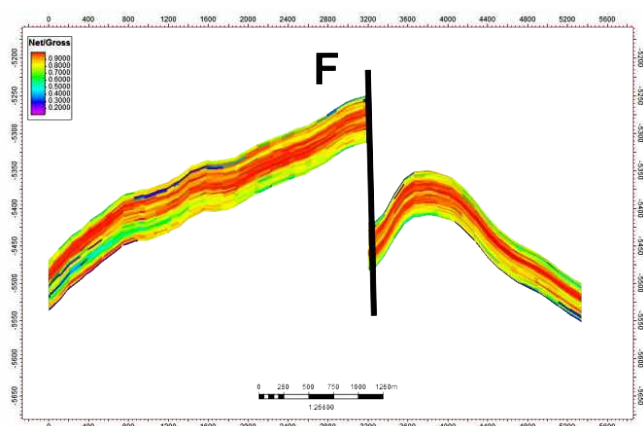


Figure 9bii: NTG model cross section of reservoir G9.

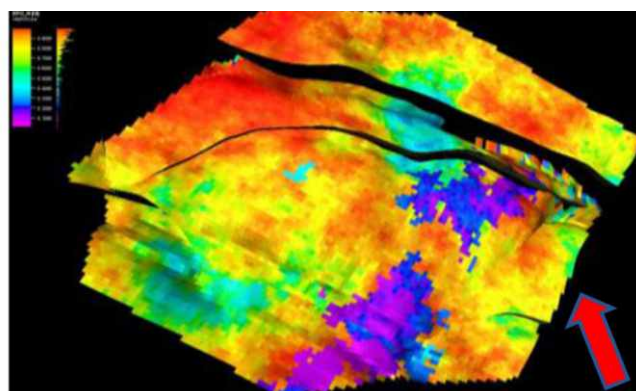


Figure 9di: NTG model of reservoir G11.

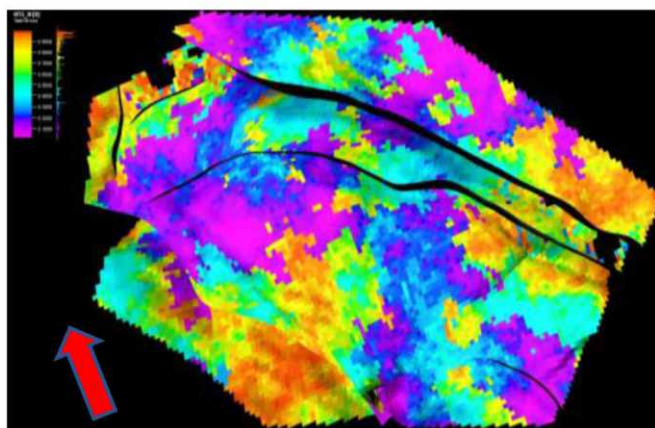


Figure 9ci: NTG model of reservoir G10.

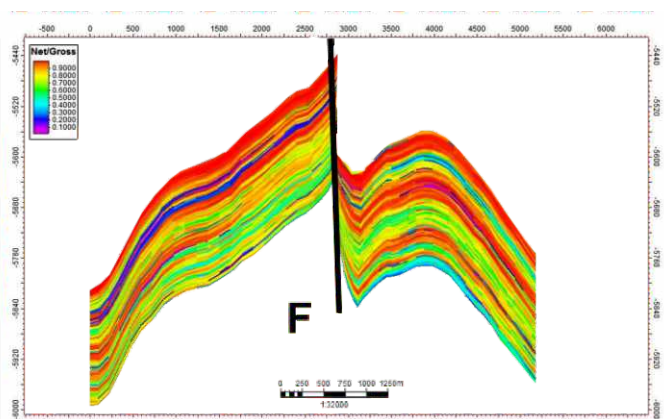


Figure 9dii: NTG model cross section of reservoir G11.

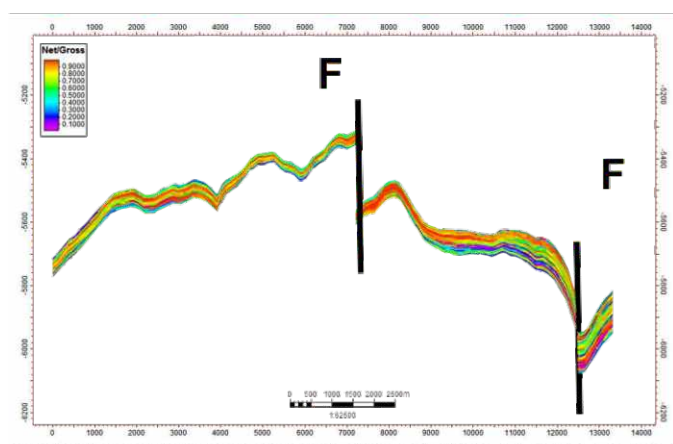


Figure 9cii: NTG model cross section of reservoir G10.

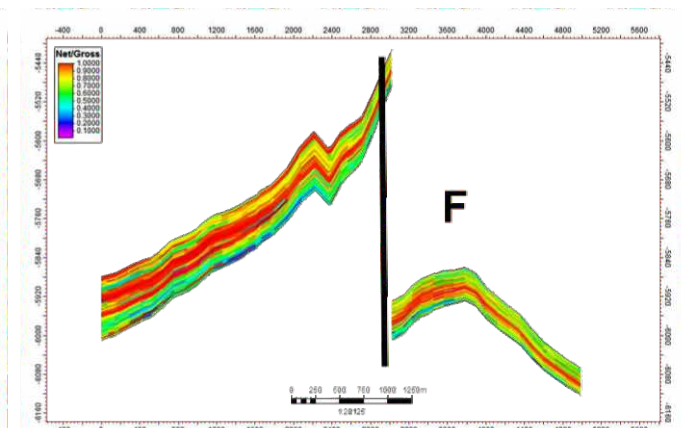


Figure 9eii: NTG model cross section of reservoir G12.

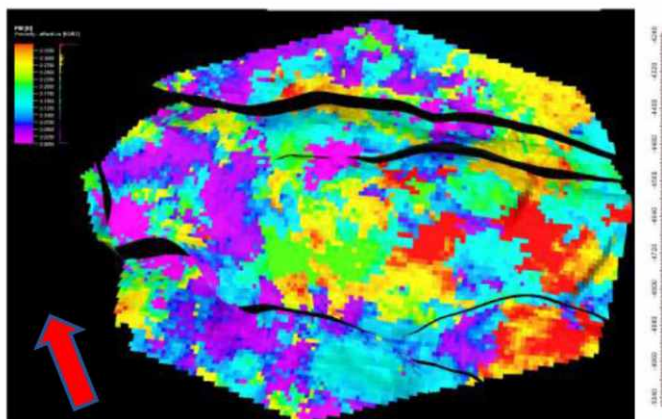


Figure 10ai: PHIE model of reservoir G1.

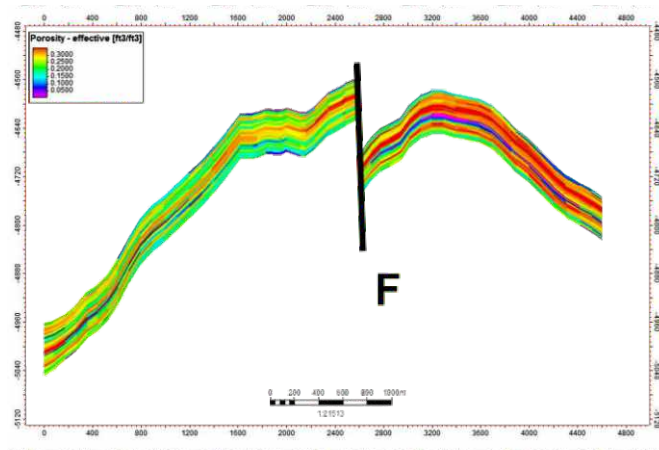


Figure. 10bii: PHIE Cross section model of reservoir G2.

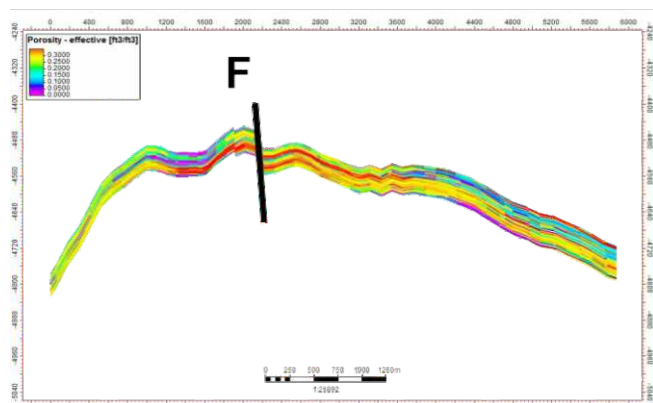


Figure 10aai: PHIE Cross section model of reservoir G1.

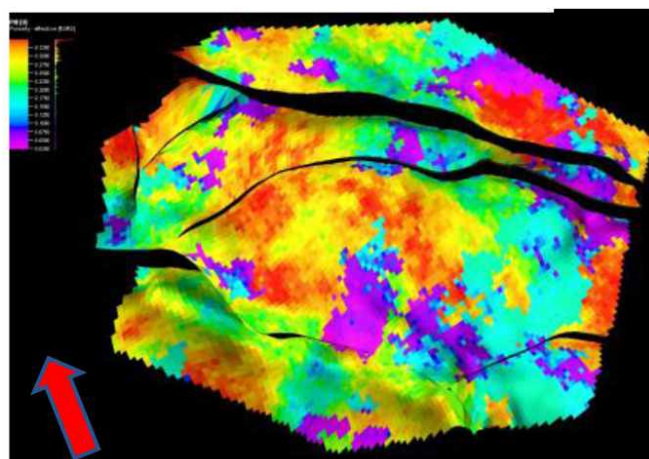


Figure 10ci: PHIE model of reservoir G9.

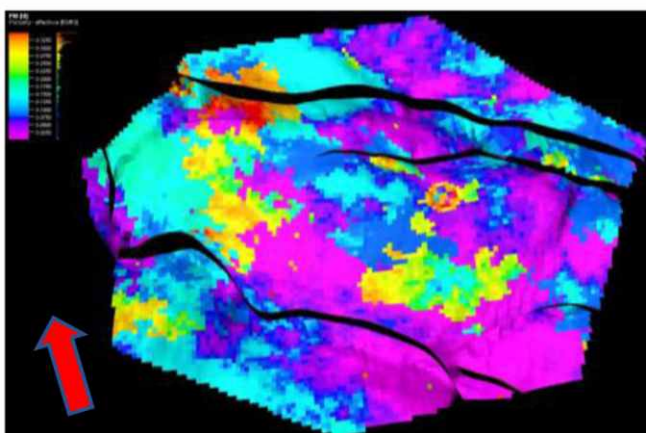


Figure 10bi: PHIE model of reservoir G2.

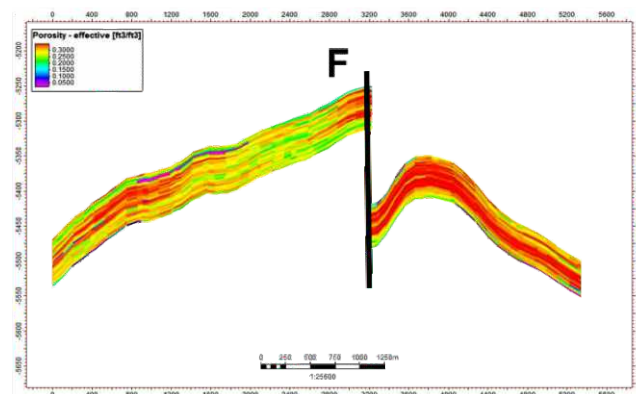


Figure 10cii: PHIE Cross section model of reservoir G9.



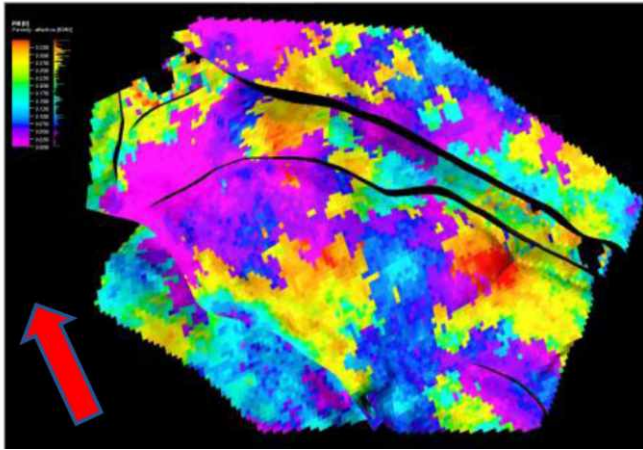


Figure 10di: PHIE model of reservoir G10.

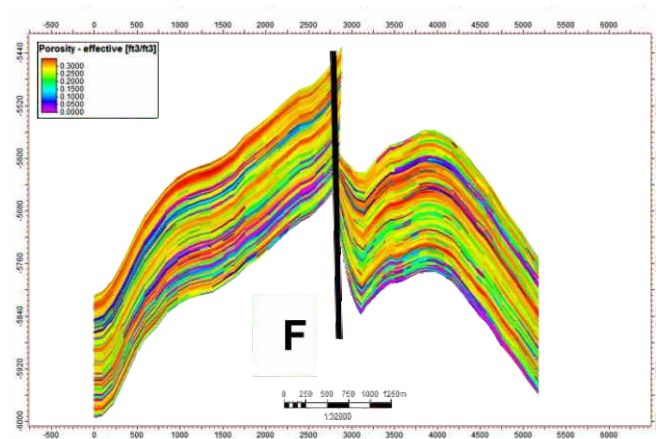


Figure 10eii: PHIE cross section model of reservoir G11.

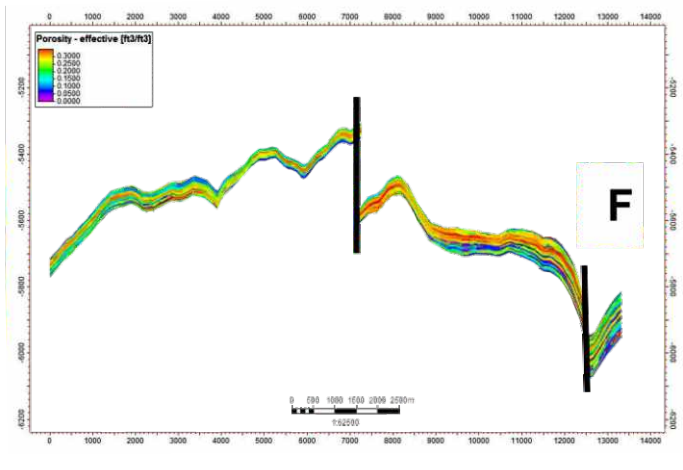


Figure 10dii: PHIE cross section model of reservoir G10.

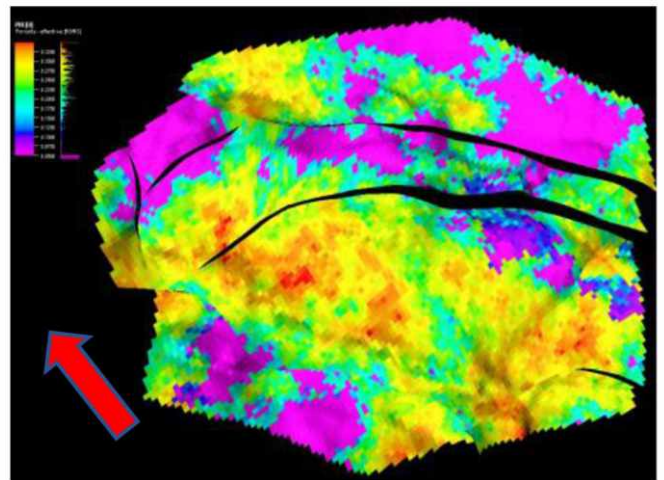


Figure 10fi: PHIE model of reservoir G12.

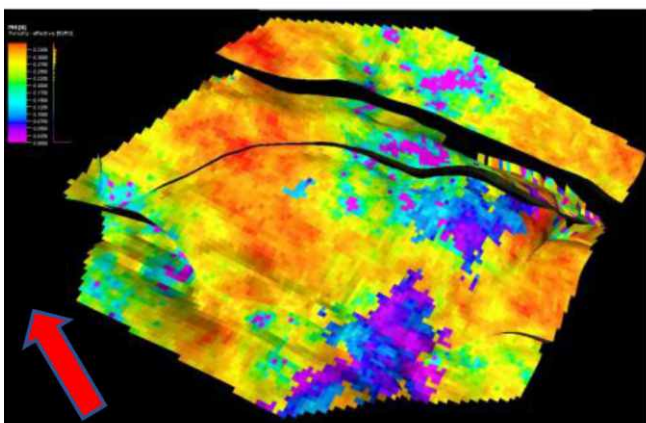


Figure 10ei: PHIE model of reservoir G11.

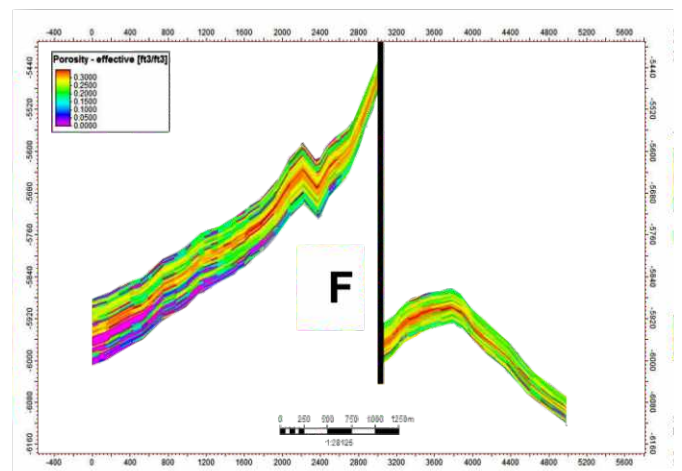


Figure 10fii: PHIE cross section model of reservoir G12.



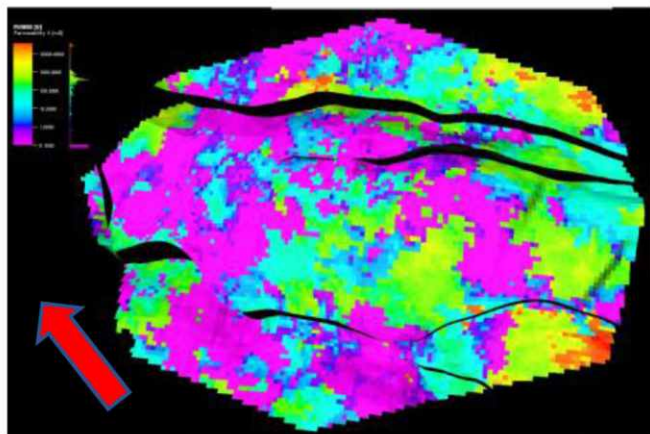


Figure 11ai: PermX model of reservoir G1.

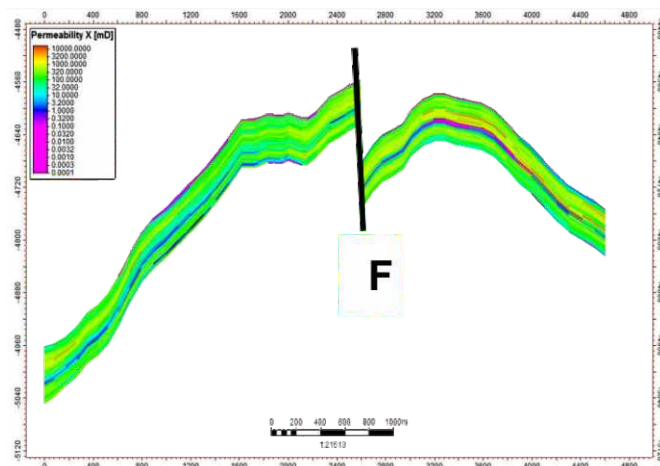


Figure 11bii: PermX Cross section model of reservoir G2.

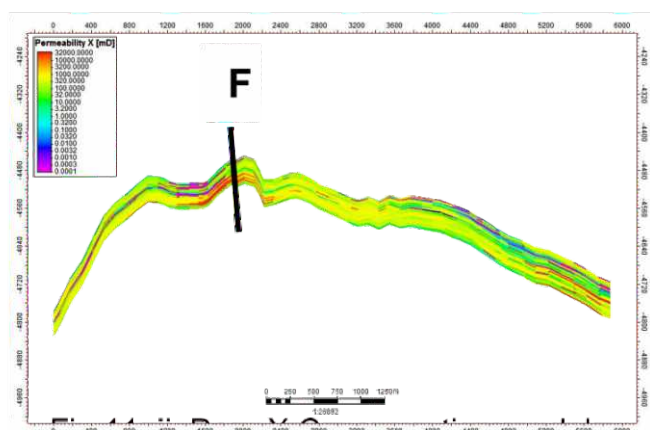


Figure 11aii: PermX Cross section model of reservoir G1.

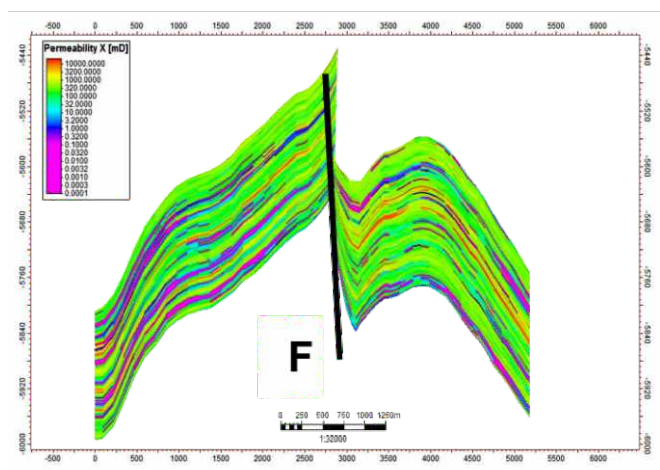


Figure 11ci: PermX Cross section model of reservoir G11.

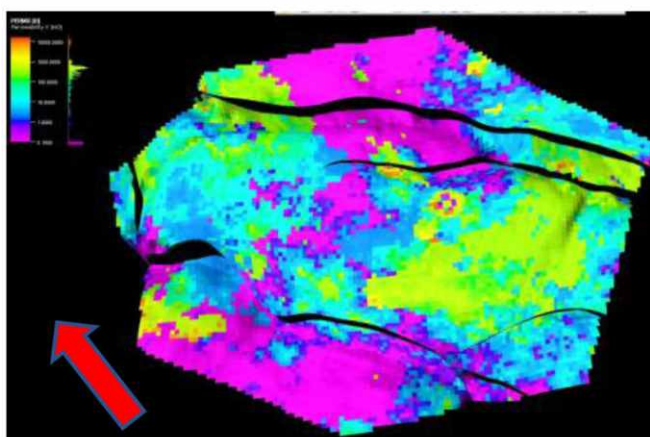


Figure 11bi: PermX model of reservoir G2.

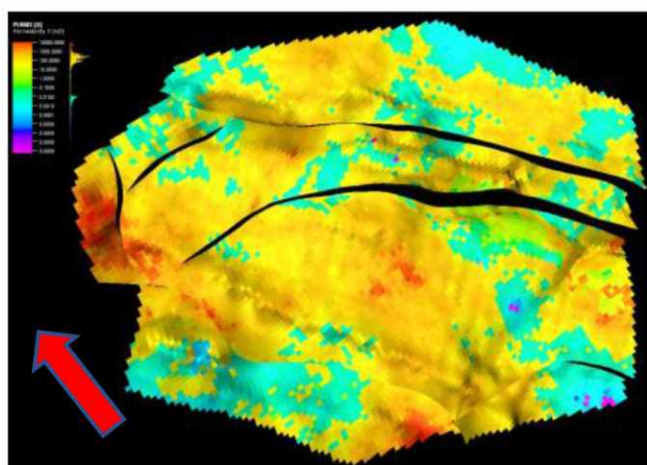


Figure 11di: PermX model of reservoir G12.

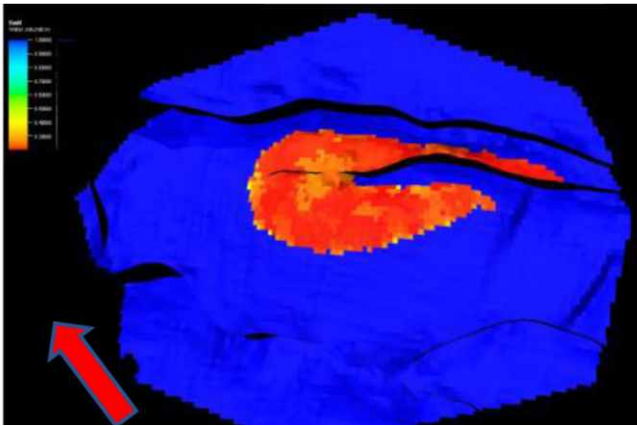


Figure 12ai: Sw model of reservoir G1.

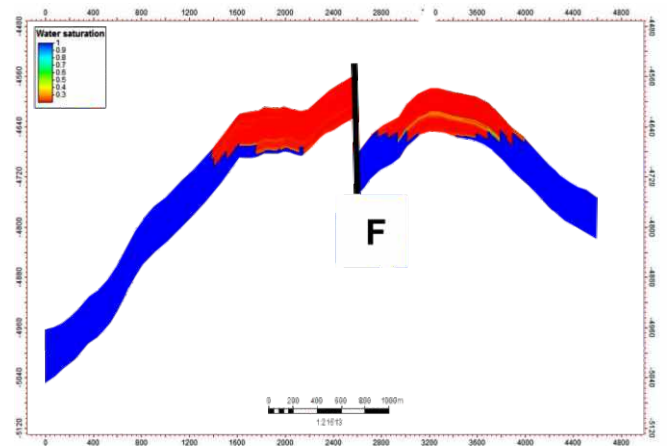


Figure 12bii: Sw cross section model of reservoir G2.

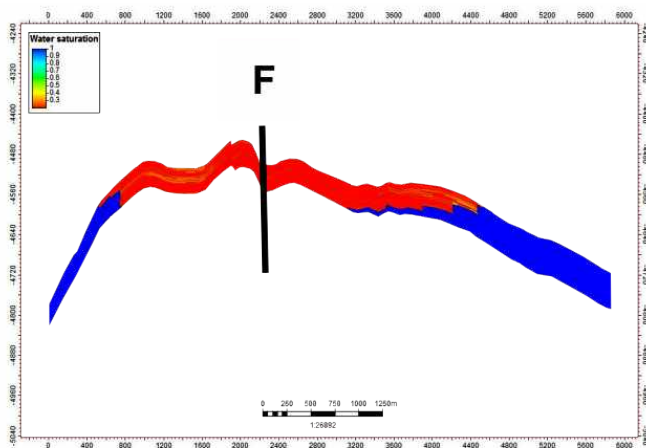


Figure 12aii: Sw cross section model of reservoir G1.

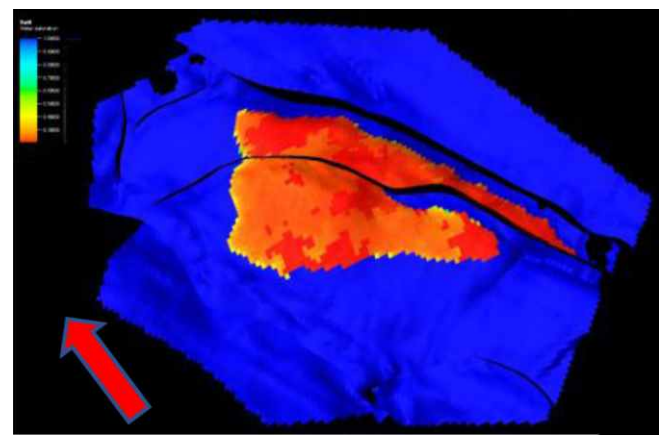


Figure 12ci: Sw model of reservoir G10.

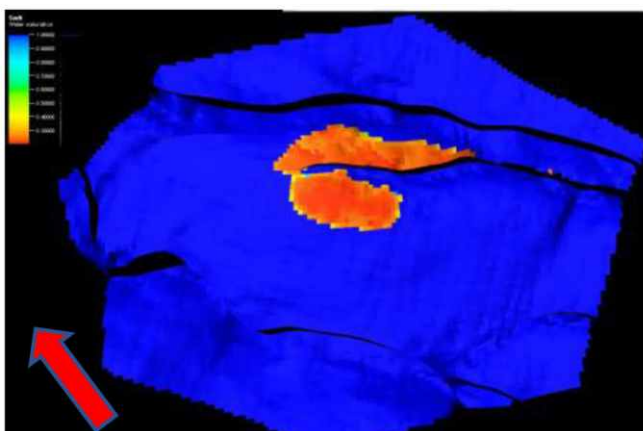


Figure 12bi: Sw model of reservoir G2.

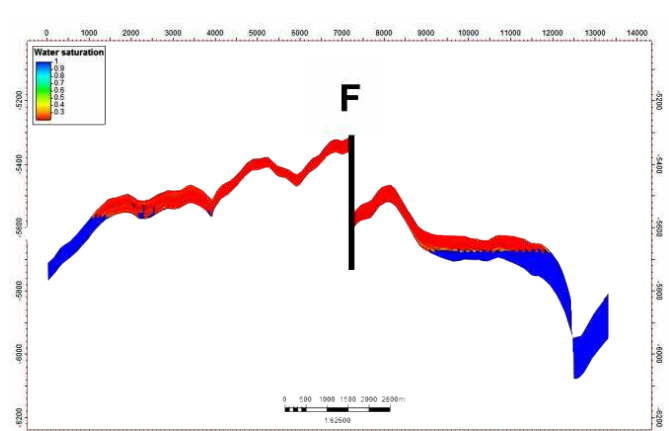


Figure 12cii: Sw cross section model of reservoir G10.

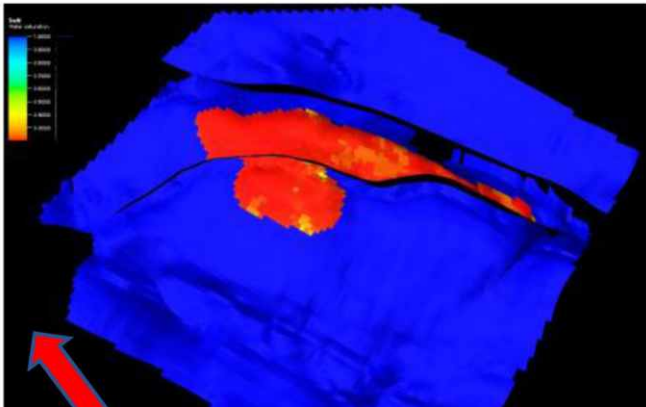


Figure 12di: Sw model of reservoir G11.

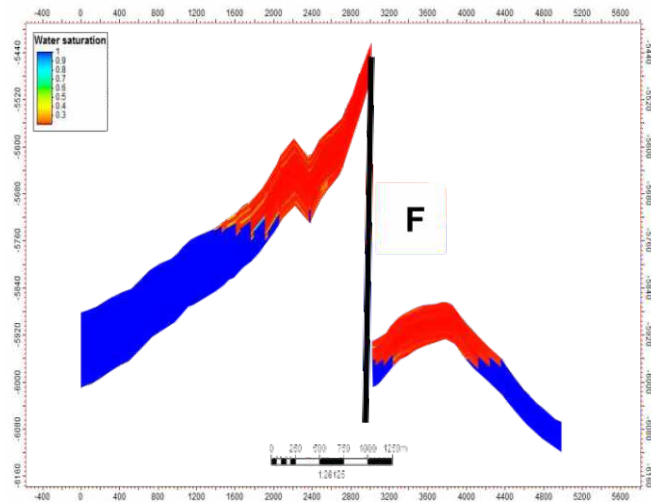


Figure 12eii: Sw cross section model of reservoir G12.

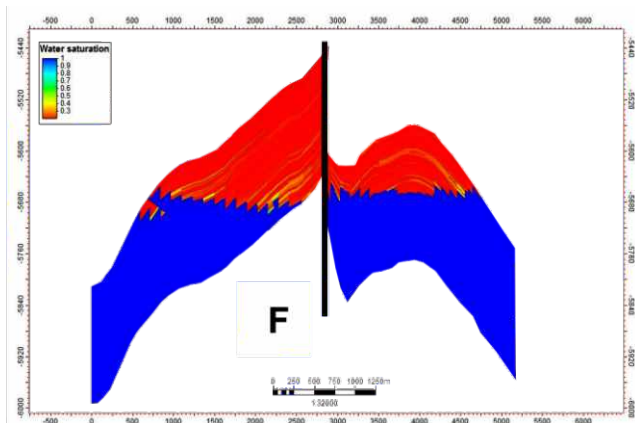


Figure 12dii: Sw cross section model of reservoir G11.

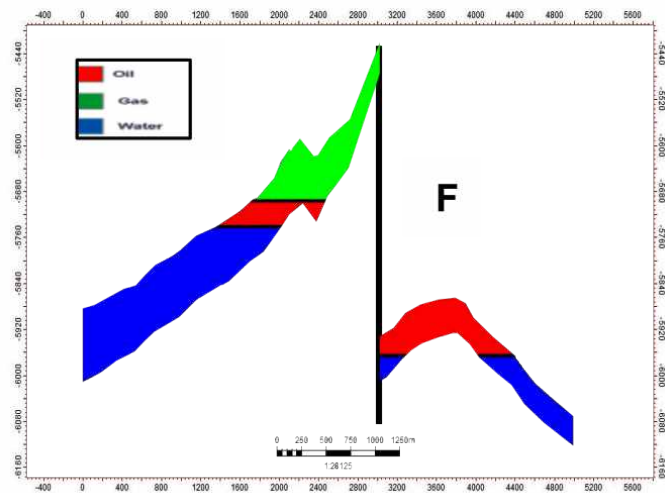


Figure 12eii: Geological cross section model of reservoir G12.

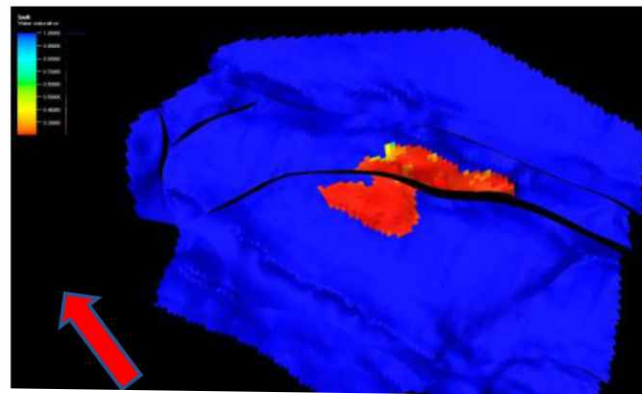


Figure 12ei: Sw model of reservoir G12.

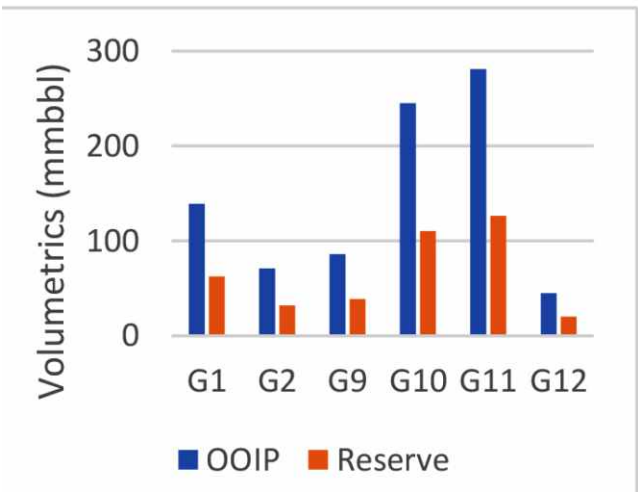


Figure 13: OOIP & Reserve within GMEDAL field.



wet in other wells. G15 and G16 reservoirs are discovered only by GMEDAL 04 and 029 wells while G17 sand was penetrated by GMEDAL 05 and 032 wells only.

GMEDAL 04 saw a GOC at 6233ft SSTVD, ODT at 6252ft in sand G15 and OWC at 6303ft SSTVD in G16 sand while GMEDAL 029 saw OWC at 6264ft SSTVD in G15 sand and is wet in G16 reservoir. Based on the petrophysical analysis done, we hereby deduced that GMEDAL 04, 011, and 029 wells are in same reservoir compartment while GMEDAL 05, 021, and 032 wells are same separate reservoir segment.

The effective porosity values within the field ranges from 23% in sand G15 to 31% in sand G5 sands while NTG ranges from 78% in G3 to 93% in G9 reservoir. The values of water saturation computed ranges from 27% in G10 to 95% in G5 sand while permeability values range from 100mD to 9500mD.

The petrophysical assessment of GMEDAL field indicated that the fluid type is gas, oil and water and favoring excellent porosity, permeability, water saturation and NTG.

### Qualitative and Quantitative Seismic Interpretation

Figure 5a-c indicate that systems of different oriented faults characterize GMEDAL field. Faults 1, 2 Fault 3 are the major faults while faults 4 to F8 are minor faults. The field is characterized by normal listric faults (F1 to F3). The faults 1-3 are trending NW-SE and are dipping SW. Both F1 and F3 runs through the entire field thereby compartmentalizing it. The F2 fault extend laterally and vertically from reservoir G1 to G12 terminating against faults F3 at this level and it causes a sealing effect on all the reservoir within GMEDAL field. The crest of the structure is separated by F2 which partly separate the crest into two at reservoir G1 and completely separate the crest at deeper reservoir G11 and G12. The throw within the field ranges 19ft at F8 in horizon G1 to 1100ft at fault F3 in horizon G12. Faults F1, F2 and F3 are extensive and parallel to each other. The parallel relationship of F1 and F3 is sustained in all reservoir levels within GMEDAL field. The field is characterized by normal fault that are listric in nature indicating Syn-depositional extensive tectonic regime. The faults F1 and F3 trending NW-SE breakup the field into Northern and Southern flanks and they control the major compartmentalization within the field.

### Reservoir Geology Modeling

Figure 6a and 6b show three parallel NW-SE trending faults (F1, F2 and F3) that control the field compartmentalization. These faults are extensive and are parallel to each other and extended from horizon G1 G12. The other faults within the field are minor in nature and also aid the field compartmentalization. The structural

model therefore conforms with and validate results of depth structure maps.

### Facies modeling

The 3D views of lithological / facies model of reservoir G1, G2, G9, G10, G11 and G12 are displayed in Figures 8ai – 8ei. The models revealed lateral distribution of sand silts and shale within GMEDAL field. The Cross-Sectional view displayed in figure 8aii – 8eii which depict the vertical lithology variation that characterized the field. Laterally, the reservoirs in GMEDAL field has better sand distribution and percentage in the order from reservoir G12, G11, G9, G10, G1 and least in G2. While only G9 has excellent sand distribution vertically across the field.

### NTG Model

The 3D view of NTG property model for all the reservoir of interest in GMEDAL field are displayed in figure 9. The model revealed excellent NTG in reservoir G12 and least in G2.

### Effective Porosity Model

Figure 10 represents the 3D model view of porosity distribution within the field. The effective porosity values were concentrated at 25% across the field and decrease southeastern ward of the field.

### Permeability Model

The 3D perspective view of permeability distribution in all the studies zones (G1, G2, G9, G10, G11 and G12) are displayed in figure 10. The permeability concentration across the field ranges from 100Md TO 1500Md which indicated that formations within GMDAL field are excellently permeable and therefore can allow free flow of fluids during production.

### Saturation Model

The 3D view of water saturation model within the field are displayed in figure 11. The saturation model revealed that water saturation ranges from about 0.1 to 0.52 within hydrocarbon bearing reservoirs. The reservoir G11 has the thickest water leg / aquifer within the field and therefore suggest that the reservoir has a strong water drive mechanism necessary for maximum production of hydrocarbon. The G12 has a gas cap of about 12ft thickness therefore oil can be produced from this level by combination drive mechanism (Figure 12eii).

### Model Contacts

The GOC, OWC and ODT observed in well penetrating different reservoirs were modeled in the 3D grid and displayed in maps and cross section (Figure 12eii).

### Quantification of Heterogeneity

The coefficient of variation of porosity from petrophysical analysis and 3D geological reservoir model

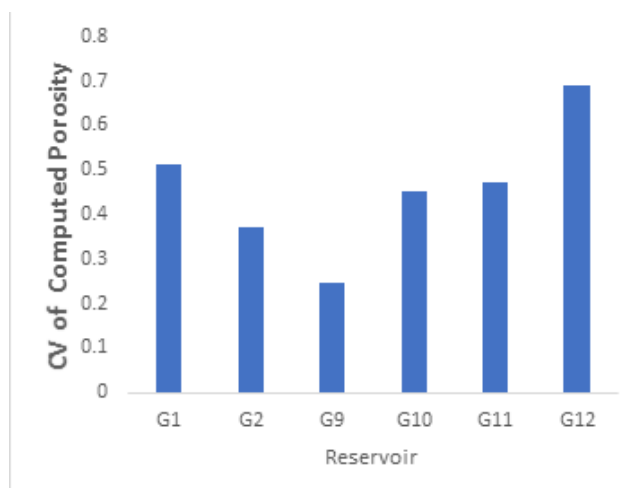


**Figure 14a:** Coeff. Of Variation for Computed Porosity.

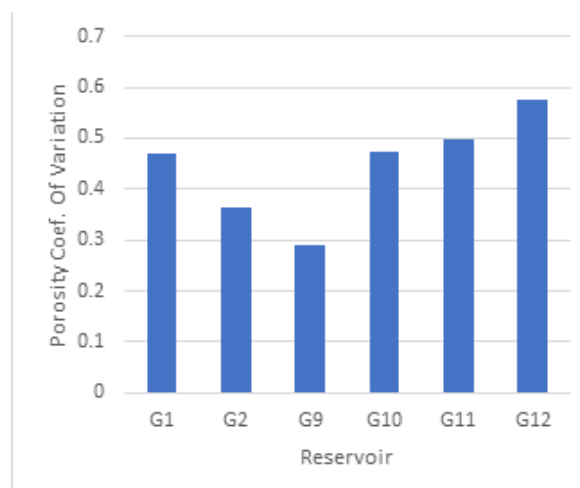


**Figure 14b:** Coeff. Of Variation for Modeled Porosity.

are presented in figure 14a and 14b. These values suggested that GMEDAL field is characterized by weak to medium intra-formational heterogeneity.

### Sedimentary Microfacies/ Environment of Deposition

The micro-facies within the field were interpreted from the GRlog motifs and NTG maps which are displayed in Figure 3a-3c. The field is characterized by distributary channel sands, shoreface and crevasse splay systems. The NTG maps indicate that the southern part of the field has low values suggesting distal environment where hydrodynamic energy of flow is low causing gradual settling of fine sand and shale deposits. The NTG maps also revealed that the field is situated in a transitional zone between proximal and distal environment i.e. coastal and marine environment.

### Model Volumetric and Reserves

The computed OOIP from all the studied reservoirs within the GMEDAL field displayed in Figure 13 revealed that reservoir G12 has the lowest OOIP of 45mmmbbl while reservoir G11 contains the highest volume of oil of about 281mmmbbl. The reservoirs G1, G2, G9, G10 and G11 are unsaturated reservoirs while G12 is saturated with gas cap of 27mmscf.

### CONCLUSION

The project and modelling of rock properties utilizing well-logs and seismic data for sand body geometry and heterogeneity delineation, geological reservoir modeling, quantification of heterogeneity and assessment of hydrocarbon beyond well control within the GMEDAL field has been done. And this research has further buttressed the efficacy of well and seismic data integration in 3D geological reservoir modelling operation.

These resulting models reveal the reservoir facies, rock properties and hydrocarbon distribution within the GMEDAL field. The petrophysical analysis of the six wells shows seventeen dominant reservoirs across the field at different depth intervals. The effective porosity values within the field range from 23% in sand G15 to 31% in sand G5 sands while NTG ranges from 78% in G3 to 93% in G9 reservoir. The values of water saturation computed range from 27% in G10 to 95% in G5 sand. The petrophysical assessment indicated that the fluid type is gas, oil and water and favoring excellent porosity, water saturation, permeability and NTG values. The field is characterized by distributary channel sands, shoreface and crevasse splay sedimentary systems situated in a transitional zone between proximal and distal environment.

The high hydrocarbon accumulation observed at the central part of the modeled reservoirs G1, G2, G9, G10, G11 & G12 are trapped by the faults (F1, F2 and F3). The trapping mechanism is therefore faults assisted three-way closure.

The discrete properties indicate facies trend in the field while continuous properties reveal petrophysical properties (effective Porosity, Permeability, Sw, and NTG) of the field. The facies trend analysis indicates that sand, silt sand and shale occur in all the modeled zones. Laterally, the reservoirs in the GMEDAL field have better sand distribution and percentage in the order from reservoir G12, G11, G9, G10, G1 and least in G2. While only G9 has excellent sand distribution vertically across the field. The model original oil in place and reserve volumes revealed that the field is hydrocarbon prolific and therefore oil can be produced in commercial quantity from all the studied reservoir levels.

Generally, the reservoirs in the GMEDAL field have weak to



medium intra-formational heterogeneity. In each of the reservoir, the net sandstone thickness, porosity, permeability and interlayer thickness exist moderate differences reflecting medium to strong interlayer heterogeneity.

## REFERENCES CITED

- Avbovbo, A. A. (1978): Tertiary Lithostratigraphy of Niger Delta. American Association of Petroleum Geologists. Bulletin, Vol. 62, p.295-306.
- Burke, et al., (1972): Longshore drift, submarine canyons, and submarine fans in development of Niger Delta: American Association of Petroleum Geologists, Vol. 56, p. 1975-1983.
- Doust, Hoker., and Omatsola, O. (1990): Niger Delta, In: Edwards J. D. and Santoyiossi, P. A. (eds.), Divergent and Passive margin basin. American Association of Petroleum Geologists, Memoir 48, p.201-238.
- De Ros et al., (1998): Heterogeneous generation and evolution of diagenetic quartzarenite in the Silurian – Devonian Furnas Formation of the Parana Basin, South Brazil. Sedimentary Geology Vol. 116, Pp 99-128.
- Evamy, B. D., Herembourne, J., Kameling, P., Knap, W. A., Molly, F. A. and Rowlands, P. H. (1978): Hydrocarbon habitat of Tertiary Niger Delta. American Association of Petroleum Geologists. Bulletin, Vol. 62, p.1-39.
- Sech et al., (2009): Three Dimensional modeling of shoreface – shelf parasequence reservoirs analogue: surface base modeling to capture high resolution facies architecture. AAPG Bulletin Vol. 93 Pp. 1155-1181.
- Schlumberger (2013): Petrel geology and Modeling, Petrel Introduction Course, 559pp.
- Short and Stauble (1967): Online Geology of Niger Delta. AAPG Bulletin. Vol. 51., Pp. 761-779.
- Weber, K. J. and Doukору, E. M (1975): Petroleum geology of the Niger Delta. Applied geology publisher Ltd.: London, UK. Vol. 2, Pp 210-221.

